

## Photoluminescence studies in epitaxial CZTSe thin films

Jan Sendler, Maxime Thevenin, Florian Werner, Alex Redinger, Shuyi Li, Carl Hägglund, Charlotte Platzer-Björkman, and Susanne Siebentritt

Citation: [Journal of Applied Physics](#) **120**, 125701 (2016); doi: 10.1063/1.4962630

View online: <http://dx.doi.org/10.1063/1.4962630>

View Table of Contents: <http://scitation.aip.org/content/aip/journal/jap/120/12?ver=pdfcov>

Published by the [AIP Publishing](#)

---

### Articles you may be interested in

[Investigation of blister formation in sputtered Cu<sub>2</sub>ZnSnS<sub>4</sub> absorbers for thin film solar cells](#)

*J. Vac. Sci. Technol. A* **33**, 061201 (2015); 10.1116/1.4926754

[Epitaxial Cu<sub>2</sub>ZnSnS<sub>4</sub> thin film on Si \(111\) 4° substrate](#)

*Appl. Phys. Lett.* **106**, 252102 (2015); 10.1063/1.4922992

[The post-growth effect on the properties of Cu<sub>2</sub>ZnSnS<sub>4</sub> thin films](#)

*J. Renewable Sustainable Energy* **7**, 011203 (2015); 10.1063/1.4908063

[Structural and optical properties of electrochemically grown highly crystalline Cu<sub>2</sub>ZnSnS<sub>4</sub> \(CZTS\) thin films](#)

*AIP Conf. Proc.* **1512**, 706 (2013); 10.1063/1.4791233

[Study of rapid thermal annealing effect on CdZnO thin films grown on Si substrate](#)


*J. Vac. Sci. Technol. B* **28**, C3D13 (2010); 10.1116/1.3374435

---

*High Energy Nanosecond Lasers*

- Energies to 1kJ
- Variable Pulsewidths
- Intuitive GUI for system control

**Continuum**<sup>®</sup>

 [www.continuumlasers.com](http://www.continuumlasers.com)

The advertisement features a black background with a photograph of a Continuum laser system. On the left is a control rack with a monitor and various buttons. In the center is a large, rectangular laser unit with a glowing yellow front panel. A red laser beam is visible at the bottom left. The text 'High Energy Nanosecond Lasers' is written in a white, italicized font at the top left. A list of features is on the right, and the Continuum logo and website are at the bottom right.

## Photoluminescence studies in epitaxial CZTSe thin films

Jan Sendler,<sup>1,a)</sup> Maxime Thevenin,<sup>1</sup> Florian Werner,<sup>1</sup> Alex Redinger,<sup>1,2</sup> Shuyi Li,<sup>3</sup> Carl Högglund,<sup>3</sup> Charlotte Platzer-Björkman,<sup>3</sup> and Susanne Siebentritt<sup>1</sup>

<sup>1</sup>Laboratory for Photovoltaics, Physics and Materials Science Research Unit, University of Luxembourg, 41 rue du Brill, 4422 Belvaux, Luxembourg

<sup>2</sup>Helmholtz-Zentrum für Materialien und Energie GmbH, Hahn-Meitner-Platz 1, D-14109 Berlin, Germany

<sup>3</sup>Ångström Solar Center, Solid State Electronics, Uppsala University, Box 534, SE-751 Uppsala, Sweden

(Received 18 May 2016; accepted 30 August 2016; published online 22 September 2016)

Epitaxial  $\text{Cu}_2\text{ZnSnSe}_4$  (CZTSe) thin films were grown by molecular beam epitaxy on GaAs(001) using two different growth processes, one containing an in-situ annealing stage as used for solar cell absorbers and one for which this step was omitted. Photoluminescences (PL) measurements carried out on these samples show no dependence of the emission shape on the excitation intensity at different temperatures ranging from 4 K to 300 K. To describe the PL measurements, we employ a model with fluctuating band edges in which the density of states of the resulting tail states does not seem to depend on the excited charge carrier density. In this interpretation, the PL measurements show that the annealing stage removes a defect level, which is present in the samples without this annealing. *Published by AIP Publishing.* [<http://dx.doi.org/10.1063/1.4962630>]

### I. INTRODUCTION

CZTSe is a suitable absorber layer in thin film photovoltaic devices. Current conversion efficiencies reach the values up to 12.6 % for the related sulfur-selenium alloy CZTSSe,<sup>1</sup> the main limitation currently being the low open circuit voltage  $V_{OC}$  when compared to the band gap  $E_G$  of the absorber.<sup>2</sup> It has been shown that grain boundaries have an effect on the material properties (see, for example, Ref. 3 or 4 for the similar chalcopyrites), so measurements on the polycrystalline absorber layers and solar cells are always influenced by grain boundaries. In order to study the undistorted properties of CZTSe, it is desirable to grow monocrystalline films.

Previously epitaxial thin films were grown by molecular beam epitaxy<sup>5,6</sup> on gallium arsenide (001) (GaAs) substrates. GaAs was chosen for epitaxial growth because the lattice mismatch between CZTSe and the substrate is about only 0.6%.<sup>7,8</sup>

In this paper, we describe the growth of the epitaxial thin films by a similar process and their characterization by photoluminescence (PL) spectroscopy.

Low temperature PL can be employed to study the transitions involving defect states that are thermally discharged at room temperature. The PL measurements with varying excitation intensity can yield information about the nature of the underlying transition. Combining temperature and intensity dependent measurements can also determine if the material is compensated.<sup>9</sup>

It was reported in previous publications that the PL emission in polycrystalline CZTSe samples (see, for example, Refs. 7 and 10) can be described by electrostatic potential fluctuations, which are a result of the compensation of the material. This attribution is based on the observation that the PL emission exhibits a blue shift in the peak position under the variation of the excitation intensity. The

explanation for this shift is that the charged defects, which cause the potential fluctuations, are gradually screened with the increasing charge carrier density.<sup>9,11,12</sup>

The broad asymmetric shape of the PL at low temperatures found in the epitaxial samples and the evolution with the increasing temperature correspond to electrostatic potential fluctuations. However, the absence of a blue shift with increasing excitation intensity at any temperature indicates that there is no screening of the potential fluctuations. We show that the PL measurements can instead be described by intensity independent fluctuating band edges with localized tail states.

### II. RECOMBINATION BASICS

This section summarizes the most important radiative recombination channels in a heavily doped, degenerate semiconductor based on the work of Levanyuk and Osipov.<sup>13</sup> Their description assumes a fluctuating band structure as

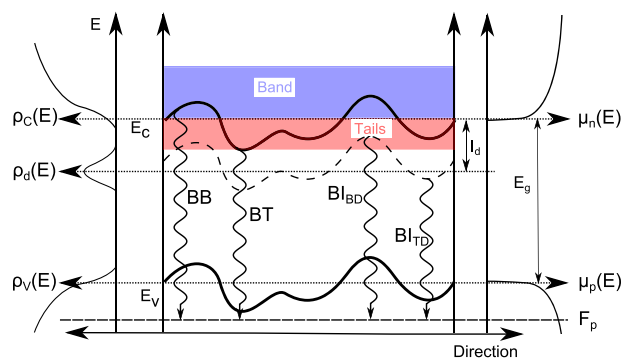


FIG. 1. Band structure and radiative recombination channels of a degenerate p-type semiconductor showing fluctuating band edges and an additional donor level. The left part of the figure shows the densities of states  $\rho$ , while the right part shows the carrier mobility. The middle part shows the different recombination channels. Due to the degeneracy, all electrons recombine into the level  $F_p$ . Adapted from Ref. 13.

<sup>a)</sup>jan.sendler@uni.lu

shown in Figure 1. This irregular potential leads to the existence of localized states, in which the charge carrier mobility is zero. They are separated from the delocalized states by the percolation levels  $E_C$  and  $E_V$  for the conduction and valence band respectively. In the following discussion, the localized states will be called tail states, while the delocalized states are denoted as band states. The degeneracy of the semiconductor causes the Fermi level  $F_p$  to lie below the localized valence band tail. This means that the majority of recombining holes in a PL experiment come from the free states, and the localized valence band tails will have no visible influence on the emission. In this case, there are three radiative recombination channels:

**Band-to-band (BB) transition:** The recombination of an electron from the delocalized conduction band states with a free hole. This process can be described by Planck's generalized law of radiation.<sup>14</sup>

**Band-to-tail (BT) transition:** The recombination of an electron in a localized conduction band tail state with a free hole. The behavior of this process under different experimental conditions is governed by the localized electron states. At low temperatures, the distribution of electrons in these states is not in a quasi-equilibrium and all localized tail states act as recombination centers. This means that the probability of radiative recombination is higher than the probability of thermal release into the band. With increasing temperature the electron distribution moves towards a quasi-equilibrium and the shallower states turn into trapping states, for which the probability of thermal release becomes bigger than the radiative recombination probability.

From this, it can be estimated that at low temperatures, the BT-transition will exhibit a red shift of the emission with increasing temperature because the demarcation level, which separates recombination and trapping centers, is shifted in the direction of the band gap. At the same time, an increase of the excitation intensity will result in a blue shift because the demarcation level is shifted in the opposite direction. This is because the probability for radiative recombination increases with the increasing charge carrier density. As soon as the electron distribution reaches a quasi-equilibrium, the BT transition shows a blue shift with increasing temperature because the energy of the state with the highest occupation is proportional to the temperature in that range. From that point, the dependence of the maximum of the emission on the rate of excitation vanishes. This situation is also observed in BB transitions where an increase of the Quasi-Fermi level splitting does not change the peak position.<sup>15</sup> Only at very high excitations, the BT transition will exhibit a blue shift as soon as all recombination centers are occupied and a further increase in excitation will turn more shallow trapping centers into recombination centers.

**Band-to-impurity (BI) transition:** If there is a localized defect level below the conduction band tails, as shown in Figure 1, an electron in this defect level can recombine with a free hole. Since these are filled by capturing electrons from the band and tail states, they can be divided into two categories: The tail defect (TD) states, which are located at positions where the corresponding band edge at the same position is a tail state and the band defect (BD) states, for

which the corresponding band edge is a band state. The TD states capture electrons from a localized tail state, while band defect states capture free electrons from the band. At low temperatures and low excitation intensities, only the TD states can be filled because under these conditions, only the localized tail states are occupied. Only at sufficiently high temperatures or excitation intensities, the BD states begin to be filled, resulting in a blue shift of the BI emission until all BD states are filled.

It should be noted that Levanyuk and Osipov discussed these transitions assuming a heavily doped semiconductor, for which the DOS might depend on the density of the excited charge carriers. However since the crucial point is the existence of localized tail states in a fluctuating band structure, this model is also applicable to an excitation independent DOS as long as it fulfils these two prerequisites.

### III. EXPERIMENTAL

The CZTSe films were grown in a molecular beam epitaxy system with a base pressure of approximately  $1 \times 10^{-8}$  Torr during growth. The system contains three elemental metal effusion cells: copper (Cu), zinc (Zn) and tin (Sn). In addition to the metal sources, a valved source with a cracking tube supplies a selenium (Se) atmosphere. A tin selenide (SnSe) effusion cell provides additional Se and counters Sn loss during growth. We used undoped epi ready gallium arsenide (GaAs) wafers (001) with a thickness of 0.5 mm as a substrate to facilitate the epitaxial growth, because the lattice mismatch between GaAs ( $a_{\text{GaAs}} = 5.653 \text{ \AA}$ )<sup>8</sup> and CZTSe in the kesterite structure ( $a_{\text{CZTSe}} = 5.605 \text{ \AA}$ )<sup>7</sup> is less than 1%. The substrate is mounted on a rotating sample holder in front of an infrared heating source with a Zn-doped GaAs backplate to enable heat transfer to the substrate. The substrate temperature was controlled with a pyrometer, which is sensitive to infrared radiation in the range from  $0.90 \mu\text{m}$  to  $0.97 \mu\text{m}$  and was set to the values between  $450^\circ\text{C}$  and  $460^\circ\text{C}$ .

The two types of growth processes are schematically depicted in Figure 2. Both processes start with a deposition stage, which lasts 45 min, during which all five sources are co-evaporating.

In the process shown in Figure 2(a), this stage is followed by an annealing step during which only the Sn, Se, and SnSe sources are open. Since the Cu source contributes significantly to the heating of the sample, the heater temperature was increased in order to keep the sample temperature during this stage close to the temperature during the growth stage. The amount of this temperature increase was varied from sample to sample. It should be noted that this *in-situ* annealing step is part of the co-evaporation process and should not be confused with a precursor-annealing process. The last step of the process is the cool-down in which the heating is turned off. During that stage, we supply a Se-flux to keep the CZTSe from decomposing. In another type of process (Figure 2(b)), the deposition stage is directly followed by the cool-down stage and the annealing stage is omitted. This was done in order to study the influence of the *in-situ* annealing stage. In the following, we will refer to the samples that were grown with the annealing stage as annealed samples, while the

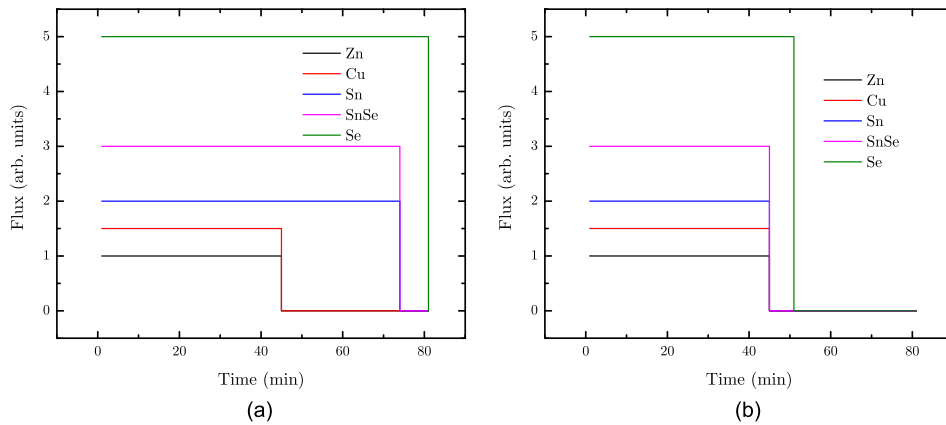


FIG. 2. Scheme of the growth processes used to grow epitaxial CZTSe samples.

samples produced with the other type of process are called not annealed. The fluxes of the five sources were measured with a beam flux monitor and a quartz crystal monitor. The fluxes were chosen such that the overall composition of the resulting films lies near the stoichiometric region of CZTSe.

After growth, one of the not annealed samples was subjected to an ordering procedure. This aims at reducing the  $\text{Cu}_{\text{Zn}}$  and  $\text{Zn}_{\text{Cu}}$  anti-sites that form above a critical temperature<sup>16</sup> and arrange in clusters.<sup>17</sup> It was found by Rey *et al.* that this temperature is around 200 °C for CZTSe.<sup>18</sup> This means that the co-evaporated samples have a high degree of disorder (a large amount of these anti-sites) after growth due to the high growth temperature. By annealing the sample at temperatures lower than 200 °C, the amount of anti-sites is decreased. Details about the ordering procedure can be found in Ref. 18.

The PL emission was excited with the 514.5 nm line of an Argon-laser which was focused onto a spot of roughly 100  $\mu\text{m}$  in diameter. The signal from the sample was collected utilizing a setup of two parabolic mirrors and coupled into a fiber. The light is then led into a monochromator and recorded with an InGaAs detector. To correct for the spectral sensitivities of the set-up, a halogen lamp with known spectrum was measured to obtain a correction function which is applied to the measured spectra. For the measurements at low temperatures, the samples were mounted into a continuous flow cryostat and cooled with liquid helium to minimum temperatures of 4.2 K. During the intensity dependent measurements, the power on the samples was varied in a range of about 2.5  $\text{Wcm}^{-2}$  to 125  $\text{Wcm}^{-2}$ . To estimate the doping density of the samples, temperature dependent Hall measurements were performed on one sample in a van der Pauw configuration.<sup>19</sup> The system consists of a conduction-cooled superconducting magnet and utilizes magnetic fields up to 9 T. Raman measurements were performed with a Renishaw inVia Raman microscope at the Luxembourg Institute of Science and Technology using excitation wavelengths of 442 nm and 532 nm. The dielectric function was determined using variable angles of incidence spectroscopic ellipsometry by J. A. Woollam at the University of Uppsala.

#### IV. RESULTS

Monocrystallinity of the samples was confirmed by X-ray diffraction and the absence of grain boundaries in the

SEM cross section images. Raman measurements showed no signal of secondary phases in samples with a smooth surface in the SEM topview. In samples with an inhomogeneous SEM topview, Raman mapping showed the presence of CuSe and ZnSe on some spots. The PL of these samples, however, showed no signal of those secondary phases. By fitting the main Raman mode with an asymmetric Lorentz profile, we found that the FWHM of this mode is smaller in the annealed samples which indicates that the annealing stage has a positive influence on the crystal quality (Figure 3).

The compositions of the samples are listed in Table I together with the substrate temperature before growth, the increase in the heater set-point case of the annealed samples, and the thickness determined from SEM cross sectional views.

In Secs. IV A and IV B, we will present the PL measurements in detail. Annealed and not annealed samples will be discussed separately.

#### A. Not-annealed samples

Figure 4 shows the typical evolution of the normalized PL signal of a not-annealed sample with temperature. There is a distinct blue-shift of the emission in the temperature

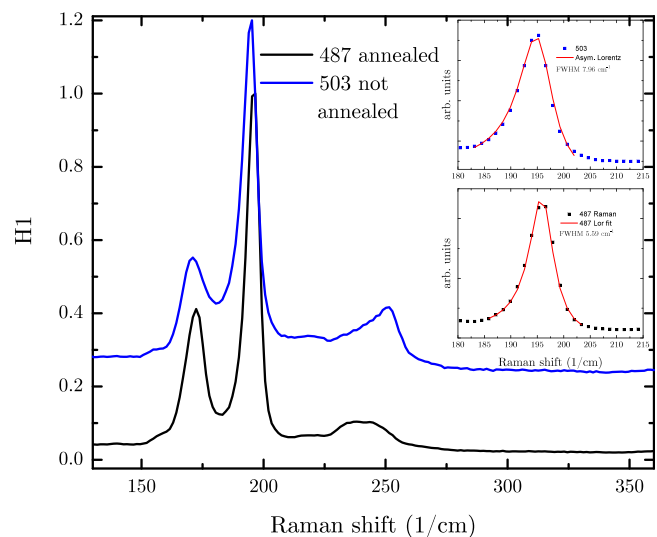


FIG. 3. 532nm Raman spectra of one annealed and one not annealed samples. The two insets show the fit of the main Raman mode with an asymmetric Lorentz profile.

TABLE I. Sample compositions determined by EDX, temperature  $T_G$  before growth, temperature increase  $\Delta T_A$  during the annealing stage and thickness  $d$ .

Sample	Anneal	Cu/(Zn + Sn)	Zn/Sn	$T_G$ (°C)	$\Delta T_A$ (°C)	$d$ ( $\mu\text{m}$ )
487	Yes	0.95	0.92	455–456	+50	1.1
490	Yes	0.91	1.08	455–456	+60	1.0
497	Yes	0.94	0.96	455–459	+40	1.1
499	No	0.91	0.89	456–461	...	1.2
506	No	0.91	0.96	451–453	...	1.2

range between 40 K and 130 K (see also Figure 5). In the same temperature range, we can observe a broadening of the peak.

To quantify this broadening, we used the following function to fit the low energy side (Eq. (2.47) (Ref. 13)):

$$I_{\text{PL}}(\hbar\omega) \propto \exp\left(-\frac{(\hbar\omega - E_0)^2}{2\gamma^2}\right). \quad (1)$$

This formula is originally used to describe the low energy side of the PL emission governed by deep potential fluctuations at low excitation intensities. In that case,  $\gamma$  is the average depth of the potential fluctuations and  $E_0$  is the energy of the transition in the unperturbed semiconductor. It also describes the low energy side of a BI transition at low temperatures and excitation rates and of BT transitions, if the carrier distribution of the tail is in a quasi-equilibrium. Figure 5 shows  $\gamma$  from the fit together with the energy of the maximum emission. From this plot, it is visible that the broadening of the low energy side happens in the same temperature range as the blue-shift of the emission.

In addition to these temperature dependent measurements, we conducted measurements with varying excitation intensity at different temperatures. At all temperatures, the peak position and the peak shape do not change with varying excitation, as it is shown in Figure 6 for 4 K. The excitation powers quoted in

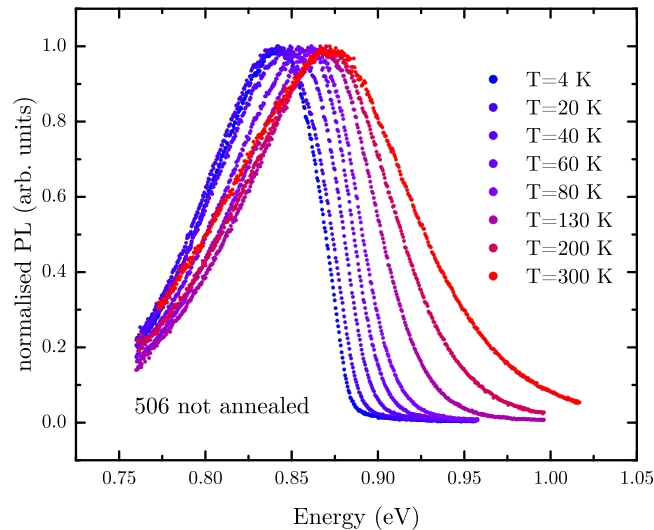


FIG. 4. Evolution of the PL emission with increasing temperature of a sample grown without the annealing stage. The spectra were taken at the same excitation intensity and are normalised to unity. For better visibility, some temperature steps are omitted.

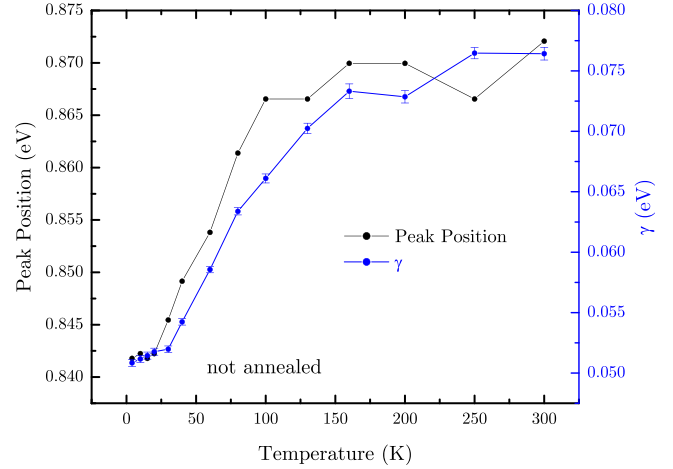


FIG. 5. Peak position and  $\gamma$  versus temperature for the not-annealed sample. The uncertainties of  $\gamma$  are taken from the fit. The lines act as a guide for the eye.

the legend correspond to the output power of the laser. The actual power on the sample scales linear with the laser power and is roughly  $2.5 \text{ W/cm}^2$  to  $125 \text{ W/cm}^2$ .

We used a power law to relate the intensity of the PL emission  $I_{\text{PL}}$  with the laser power  $I_L$ <sup>9</sup>

$$I_{\text{PL}} \propto I_L^k. \quad (2)$$

Figure 7 shows a plot of the logarithm of the PL intensity versus the logarithm of the excitation intensity. In this representation, the exponent  $k$ , or the  $k$ -value, can be extracted from a linear fit. From this plot, we can see that the  $k$ -value lies close to 1 at all temperatures with the exception of the measurement at 4 K.

## B. Annealed samples

In the annealed samples, we observe two different kinds of behavior, which are exemplarily shown in Figures 8 (labelled type 1) and 9 (labelled type 2). The low temperature emission of type 1 sample is at lower energies compared

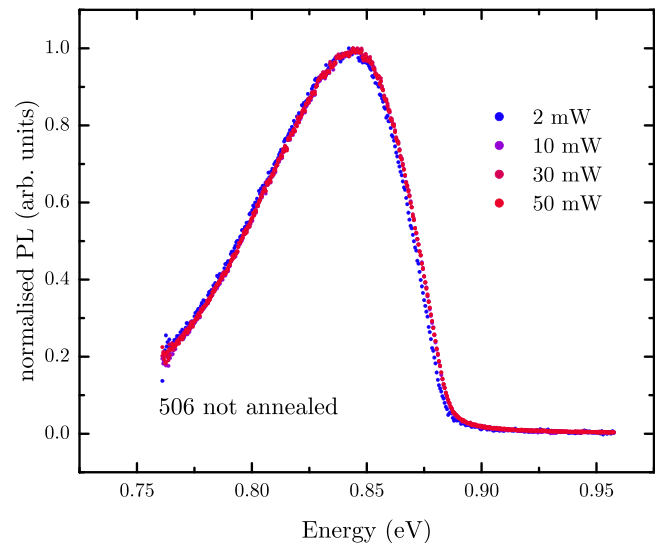


FIG. 6. Normalised PL spectra of the not annealed sample at 4 K and varying excitation intensity.

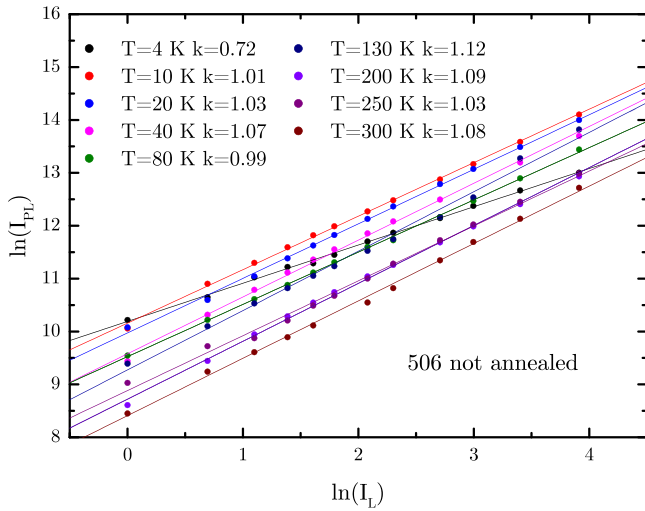


FIG. 7. K-values for the not annealed sample determined with Equation (2).  $I_{PL}$  is obtained by integrating over the spectra.

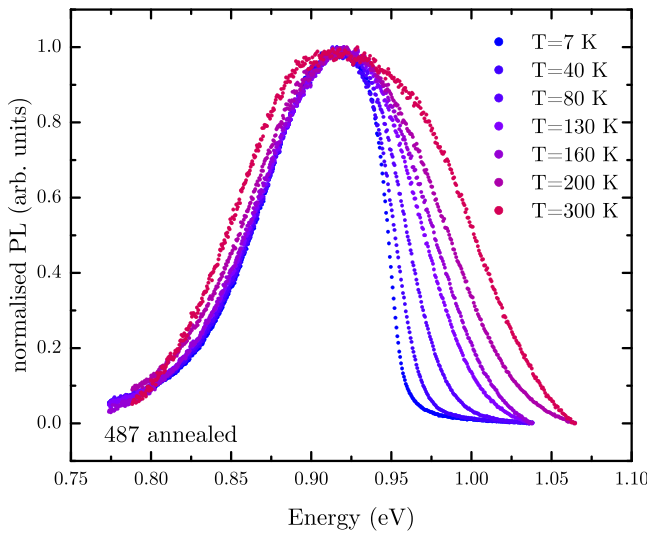


FIG. 8. Evolution of the PL emission with increasing temperature of an annealed sample showing type 1 behavior.

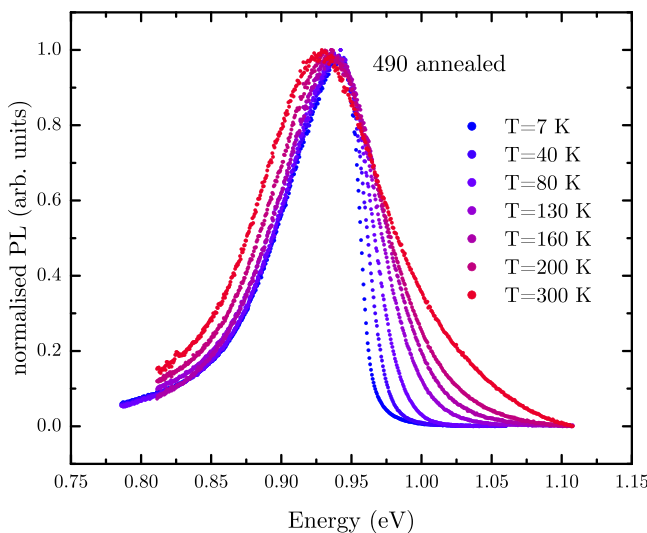


FIG. 9. Evolution of the PL emission with increasing temperature of an annealed sample showing type 2 behavior.

to type 2 sample. With increasing temperature, it exhibits a broadening on the high energy side, which is not present in type 2 sample. In contrast to the not annealed samples, there is only a weak blue shift in type 1 sample and a red-shift in type 2 sample with temperature and no pronounced broadening of the low energy side in the annealed samples.

The evolution of the quantity  $\gamma$  and of the peak position with temperature for the two samples is shown in Figures 10 and 11 (note the smaller scale for  $\gamma$  compared to Figure 5). From the peak position, we can see that type 1 sample exhibits a blue-shift at low temperatures which turns into a red-shift at around 130 K, while  $\gamma$  increases monotonically. In the case of type 2 sample, we observe a red-shift only, while  $\gamma$  remains essentially constant.

As for the not annealed samples, the exponent  $k$  (Equation (2)) assumes values very close to 1 and the peak shape remains unchanged with the increasing excitation intensity at all temperatures for both samples (not shown here).

### V. DISCUSSION

Temperature dependent Hall measurements on one annealed sample show an effective doping density in the order of  $10^{20} \text{ cm}^{-3}$ . This high level of doping implies that the sample is degenerate and that the valence band tail states do not have a significant influence on the PL. Assuming that this is the case for all samples, the PL emission can be assigned in the following manner.

The PL emission in the not annealed samples can be attributed to a BI transition. The large blue-shift correlates with the broadening of the peak with increasing temperature, which is then a result of the filling of the BD states as soon as the temperature is high enough. The blue-shift and the broadening cease when all BD states are occupied. In this case, the low energy side of the emission is characterized by  $\gamma$  at low temperatures<sup>13</sup> before the filling of the BD states, so the value for  $\gamma$  obtained by the fit can be used as a measure to estimate the depth of the potential fluctuations. For sample 506 shown in Figure 5, we obtain a value of 51 meV for  $\gamma$  at 4 K (see Table II). For sample 499, which has a slightly

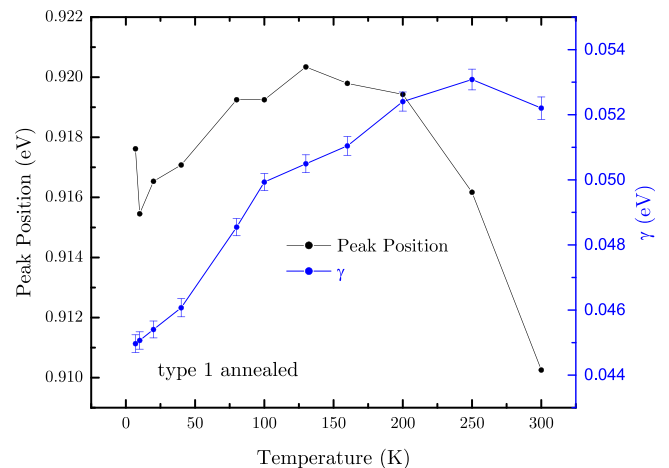


FIG. 10. Peak position and  $\gamma$  versus temperature for the annealed sample with type 1 behavior. The uncertainties of  $\gamma$  are taken from the fit. The lines act as a guide for the eye.

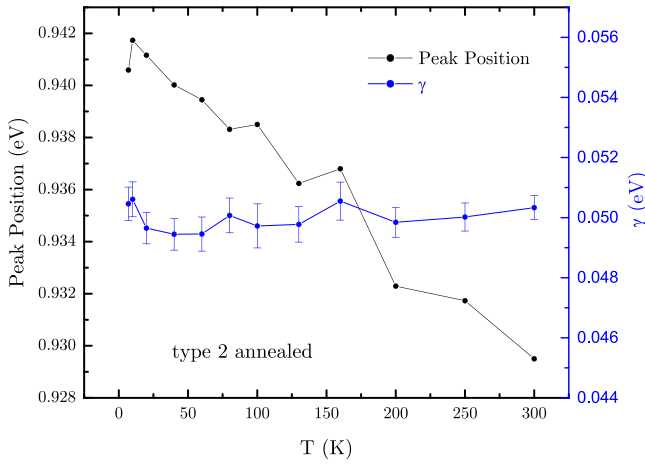


FIG. 11. Peak position and  $\gamma$  versus temperature for the annealed sample with type 2 behavior. The uncertainties of  $\gamma$  are taken from the fit. The lines act as a guide for the eye.

lower zinc content, we find  $\gamma = 44$  meV at 4 K. This sample was subjected to an ordering procedure which increases the band gap, as determined by ellipsometry, by 40 meV compared to the as grown sample, but the value for  $\gamma$  remains unchanged. This leads to the conclusion that the  $\text{Cu}_{\text{Zn}} + \text{Zn}_{\text{Cu}}$  defect clusters do not have a significant influence on the fluctuation depth in this sample. The maximum  $I_d$  of the defect DOS  $\rho_d(E)$  (see Figure 1) can be determined at low temperatures as<sup>13</sup>

$$I_d = E_G - E_{\text{max}}^{\text{BI}}. \quad (3)$$

Here,  $E_{\text{max}}^{\text{BI}}$  is the maximum of the PL emission and  $E_G$  is the band gap defined by the percolation levels. The exact value of  $E_G$  for these samples is unknown, but spectroscopic ellipsometry measurements (see Table II) indicate that it lies between 1 eV and 0.94 eV for the not annealed samples. In this case, we can estimate the ionization energy of the donor to be in the order of  $I_d \approx 100$  meV. The magnitude of the blue-shift can be related to the energy difference between the undistorted conduction band edge  $E_c^0$  and the percolation level  $E_c$  in the following:<sup>13</sup>

$$\Delta E_c = E_c^0 - E_c. \quad (4)$$

For sample 499, we obtain values of 17 meV and 20 meV after the ordering procedure. For sample 506, which shows a bigger fluctuation depth, we also obtain a higher value of 30 meV for  $\Delta E_c$ . This correlation is expected because the

TABLE II. Average fluctuation depth  $\gamma$  at the lowest measurement temperature,  $\Delta E_c$  for the not annealed samples and band gap  $E_G^{\text{ellips}}$  determined by spectroscopic ellipsometry.

Sample	Anneal	$\gamma$ (meV)	$\Delta E_c$ (meV)	$E_G^{\text{ellips}}$
487	Yes	45	...	0.91
497	Yes	54	...	...
499 as grown	No	44	17	0.86
499 ordered	No	44	20	0.90
506	No	51	30	0.97

larger fluctuation depth indicates that the DOS below the undistorted conduction band edge is higher in this sample and consequently the percolation level penetrates deeper into the band gap.

The PL emission of the annealed samples at low temperatures can be assigned to a BT transition. In the samples labelled with type 1, an additional BB transition appears at higher temperatures. The BT transition manifests itself in the blue-shift and the broadening of the emission with increasing temperature. Furthermore, the absence of a change in the peak shape with increasing excitation indicates that the carrier distribution in the tail states is in quasi-equilibrium. In this temperature range, the BT transition can also show a blue-shift itself with increasing temperature or excitation. The broadening of the PL signals due to the emerging BB transition with increasing temperature leads to an increase of  $\gamma$ , as obtained by the fit. Therefore, it can be related to the fluctuation depth only at low temperatures, when the main contribution to the PL comes from the BT transition. The red-shift starting from 160 K can be explained by thermal narrowing of the band gap.<sup>20</sup> Type 2 samples show only a BB transition at all temperatures. This conclusion is drawn from the fact that  $\gamma$  remains virtually constant, indicating that the underlying DOS does not change with temperature. This implies that  $\gamma$  cannot be related to the fluctuation depth for these samples. At the same time, the peak position is decreasing monotonically, which can again be explained by thermal narrowing of the band gap.

Using Equation (1) to fit the low energy side of the BT transition at low temperatures (assuming that the BB transition does not have a significant influence on the slope in this range) yields values of around 50 meV for  $\gamma$ , which is comparable to the not annealed samples. This indicates that the annealing stage does not influence the average potential depth but it appears to remove the defect level that was found in the not annealed samples. The values obtained for  $\gamma$  are summarized in Table II. Note that sample 490 is missing because its PL emission is assigned to a BB transition, for which  $\gamma$  is not a meaningful quantity.

Further information can be extracted from the observation that the  $k$ -value (Equation (2)) is 1 for all temperatures and samples, except for the 4 K measurement of the not-annealed sample.

It can be shown<sup>21,22</sup> that the luminescence intensity in a system with only two states, which are far from being completely occupied, grows linearly with the excitation rate; in other words for such a system,  $k = 1$  (Equation (2)) is expected. Only as soon as one of the participating states is getting close to saturation or if there is an intermediate state, which is filled by capturing carriers from one of the two states contributing to the luminescence, the  $k$ -value will deviate from 1. Taking this into account for our measurements, we can see that we have a transition between two states, which are not saturated in both the annealed and the not-annealed samples. In both cases, there is no visible influence of an intermediate state, indicating that these samples do not exhibit a significant amount of deep defect levels as it has been observed in certain CZTSe samples.<sup>23</sup>

## VI. SUMMARY

In this study, we investigated single crystal CZTSe samples grown by the molecular beam epitaxy with and without an *in-situ* annealing stage. We could show through excitation intensity and temperature dependent PL measurements that these samples can be described by a fluctuating band structure, which causes the presence of delocalized tail states. The absence of a blue-shift with increasing excitation intensity in all samples at all temperatures indicates that there is no visible influence of the carrier concentration on the DOS. This can mean that the DOS is intrinsically independent of the carrier concentration, as would be the case in band gap fluctuations. Another possibility is that the fluctuations are caused by electrostatic potential fluctuations after all, but that the doping concentration is so high that screening by excited charge carriers does not have a significant influence. Therefore, the underlying reason for the fluctuating band structure cannot be conclusively resolved. In the not annealed samples, we observed a defect level of about 100 meV below the conduction band, which was not found in the annealed samples. Furthermore, we found that an ordering procedure applied to a not annealed sample did not change the average fluctuations depth  $\gamma$ . This might be a hint that the  $\text{Cu}_{\text{Zn}} + \text{Zn}_{\text{Cu}}$  clusters, which are partly removed by the ordering procedure, do not play a major role for the formation of the fluctuating band structure.

## SUPPLEMENTARY MATERIAL

See [supplementary material](#) for SEM top view and cross sectional images of one annealed and one not annealed samples and their X-ray diffractograms.

## ACKNOWLEDGMENTS

We would like to acknowledge the Kestcells project FP7-PEOPLE-2012-ITN-316488 and the KITS2 project for funding. Furthermore, we would like to thank the Luxembourg Institute of Science and Technology for using

their scanning electron microscope, their energy dispersive X-ray spectroscopy, and their Raman microscope.

- <sup>1</sup>W. Wang, M. T. Winkler, O. Gunawan, T. Gokmen, T. K. Todorov, Y. Zhu, and D. B. Mitzi, *Adv. Energy Mater.* **4**, 1301465 (2014).
- <sup>2</sup>S. Siebentritt, *Thin Solid Films* **535**, 1 (2013).
- <sup>3</sup>J. B. Li, V. Chawla, and B. M. Clemens, *Adv. Mater.* **24**, 720 (2012).
- <sup>4</sup>U. Rau, K. Taretto, and S. Siebentritt, *Appl. Phys. A* **96**, 221 (2009).
- <sup>5</sup>A. Redinger, R. Djemour, T. P. Weiss, J. Sendler, S. Siebentritt, and L. Gütay, in *Proceedings of the 2013 IEEE 39th Photovoltaic Specialists Conference (PVSC)* (2013), pp. 0420–0425.
- <sup>6</sup>A. Redinger, H. Groiss, J. Sendler, R. Djemour, D. Regesch, D. Gerthsen, and S. Siebentritt, in *Proceedings of the E-MRS 2014 Spring Meeting, Symposium A, Thin-Film Chalcogenide Photovoltaic Materials* [Thin Solid Films **582**, 193 (2015)].
- <sup>7</sup>S. Siebentritt and S. Schorr, *Prog. Photovoltaics: Res. Appl.* **20**, 512 (2012).
- <sup>8</sup>J. S. Blakemore, *J. Appl. Phys.* **53**, R123 (1982).
- <sup>9</sup>S. Siebentritt and U. Rau, in *Wide-Gap Chalcopyrites*, edited by R. Hull, R. Osgood, J. Parisi, and H. Warlimont (Springer, 2006), Chap. 7.
- <sup>10</sup>M. Yakushev, I. Forbes, A. Mudryi, M. Grossberg, J. Krustok, N. Beattie, M. Moynihan, A. Rockett, and R. Martin, in *Proceedings of the E-MRS 2014 Spring Meeting, Symposium A, Thin-Film Chalcogenide Photovoltaic Materials* [Thin Solid Films **582**, 154 (2015)].
- <sup>11</sup>P. W. Yu, *J. Appl. Phys.* **48**, 5043 (1977).
- <sup>12</sup>B. Shklovskii and A. Efros, in *Electronic Properties of Doped Semiconductors*, edited by M. Cardona, P. Fulde, and H.-J. Queisser (Springer-Verlag, 1984).
- <sup>13</sup>A. P. Levanyuk and V. V. Osipov, *Phys.-Usp.* **24**, 187 (1981).
- <sup>14</sup>P. Würfel, *Physics of Solar Cells* (Wiley-VCH, 2005).
- <sup>15</sup>L. Gütaytay and G. Bauer, in *Proceedings of the Thin Film Chalcogenide Photovoltaic Materials (EMRS, Symposium L)* [Thin Solid Films **517**, 2222 (2009)].
- <sup>16</sup>S. Schorr, *Sol. Energy Mater. Sol. Cells* **95**, 1482 (2011).
- <sup>17</sup>S. Chen, A. Walsh, X.-G. Gong, and S.-H. Wei, *Adv. Mater.* **25**, 1522 (2013).
- <sup>18</sup>G. Rey, A. Redinger, J. Sendler, T. P. Weiss, M. Thevenin, M. Guennou, B. El Adib, and S. Siebentritt, *Appl. Phys. Lett.* **105**, 112106 (2014).
- <sup>19</sup>L. J. van der Pauw, *Philips Tech. Rev.* **20**, 220 (1958).
- <sup>20</sup>S. Choi, T. Kim, S. Hwang, J. Li, C. Persson, Y. Kim, S.-H. Wei, and I. Repins, *Sol. Energy Mater. Sol. Cells* **130**, 375 (2014).
- <sup>21</sup>T. Schmidt, K. Lischka, and W. Zulehner, *Phys. Rev. B* **45**, 8989 (1992).
- <sup>22</sup>W. Grieshaber, E. F. Schubert, I. D. Goepfert, R. F. Karlicek, M. J. Schurman, and C. Tran, *J. Appl. Phys.* **80**, 4615 (1996).
- <sup>23</sup>T. P. Weiss, A. Redinger, D. Regesch, M. Mousel, and S. Siebentritt, *IEEE J. Photovoltaics* **4**, 1665 (2014).